Giant Tunability of Intersubband Transitions and Quantum Hall Quartets in Ultrathin InSe Quantum Wells

Dmitry Shcherbakov[1*], Greyson Voigt[1], Shahriar Memaran[2,3], Gui-Bin Liu[4], Qiyue Wang[5], Kenji Watanabe[6], Takashi Taniguchi[7], Dmitry Smirnov[2], Luis Balicas[2,3], Fan Zhang[5], Chun Ning Lau[1†]

[1] Department of Physics, The Ohio State University, Columbus, OH 43221.

[2] National High Magnetic Field Laboratory, Tallahassee, FL 32310

[3] Department of Physics, Florida State University, Tallahassee, FL 32306

[4] School of Physics, Beijing Institute of Technology, 100081 Beijing, China

[5] Department of Physics, The University of Texas at Dallas, 800 West Campbell Road, Richardson, Texas 75080-3021, USA

[6] Research Center for Electronic and Optical Materials, National Institute for Materials Science, 1-1 Namiki, Tsukuba 305-0044, Japan

[7] Research Center for Materials Nanoarchitectonics, National Institute for Materials Science, 1-1 Namiki, Tsukuba 305-0044, Japan

Abstract

A two-dimensional (2D) quantum electron system is characterized by the quantized energy levels, or subbands, in the out-of-plane direction. Populating higher subbands and controlling the inter-subband transitions have wide technological applications such as optical modulators and quantum cascade lasers[1]. In conventional materials, however, the tunability of intersubband spacing is limited. Here we demonstrate electrostatic population and characterization of the second subband in few-layer InSe quantum wells, with giant tunability of its energy, population, and spin-orbit coupling strength, via the control of not only layer thickness but also out-of-plane displacement field. A modulation of as much as 350% or over 250 meV is achievable, underscoring the promise of InSe for tunable infrared and THz sources, detectors and modulators.

In a conventional quantum well (QW), charge carriers are confined in a mesoscopic layer whose thickness is comparable to their de Broglie wavelength. The advent of 2D van der Waals (vdW) materials enables a new class of QWs that can be atomically thin, widely tunable by a number of knobs, mechanically flexible and compatible with surface probes. However, to date most electronic and optoelectronic studies of 2D vdW materials focus on the properties of the lowest electronic subband. Recently, there has been increasing interest in exploring inter-subband transitions via infrared nano-imaging[2], photo- and electro-luminescence[3] and resonant tunneling[4, 5] studies. Yet a systematic characterization and *control* of the second subband and the intersubband transition in 2D vdW semiconductors has been lacking to date.

Here we demonstrate electrostatically induced population of the second subband in InSe field effect transistors that are 7-10 layers thick, and extract the effective mass of the charge

---

carriers and the strength of the Rashba spin-orbit coupling (SOC) of the subbands from quantum oscillations, which are supported by our first-principle calculations. For a given thickness L, the energetic spacing between the first and second subbands E_{12} scales quadratically with $E_\perp$, with a tunability coefficient that increases with L; as L varies, their minimum spacing scales as $1/L^2$. At high magnetic fields, the simultaneous occupation of two subbands, together with the helical spin degrees of freedom, leads to the formation of electronic quartets in the quantum Hall regime, where the ring-shaped crossings between Landau levels from the two subbands reveal a series of quantum phase transitions between paramagnetic and helical magnetic states.

InSe is a layered semiconductor with a layer-dependent band gap, large photoresponsivity [6-9], large gate-tunable Rashba spin-orbit coupling[10-12], high mobility[10, 13-16], and high saturation current[14]. Large-scale synthesis has been demonstrated[12, 17, 18]. In this work, devices are fabricated by encapsulating few-layer InSe sheets between hexagonal BN (hBN) layers, which are etched into Hall bar geometry and coupled to few-layer graphene electrodes[10, 13]. An Al_2O_3/Au top gate is deposited on the channel region, and the SiO_2/Si substrate serves as a back gate. Here we focus on InSe sheets that are 7 to 10 layers thick, which are sufficiently thick to enable the second subband to be populated via electrostatic gating, but sufficiently thin to function as a single narrow quantum well (as opposed to wide quantum wells that host two separate 2D electron gases on top and bottom surfaces[19]). All data are taken at 300 mK unless otherwise specified.

Fig. 1a-c plots the differentiated longitudinal resistance dR/dn (where n is the carrier density) from three different regions of a single InSe sheet, which are 6, 7 and 8-layer thick, respectively, as a function of the perpendicular magnetic field B and the charge density n_{tg} induced by the top gate, while the back gate voltage is maintained at 75V. At low densities, we observe prominent Shubnikov de Haas (SdH) oscillations arising from a single Landau fan in all three regions. In the two thicker regions, additional sets of oscillations emerge at higher densities, indicating that the Fermi level reaches the second subband (Fig. 1b-c). The electronic band structures of 7-layer InSe obtained by first-principles calculations, shown in Fig. 1e, indeed feature the presence of subbands and Rashba SOC. The onset charge density for reaching the second subband, n_{on}, is strongly thickness dependent. Fig. 1d plots n_{on} versus $1/L^2$ for six devices of different thicknesses, whose data points can be fitted to a straight line. This is expected from the classic particle-in-a-box model, in which the energetic separation E_{12} between the first two subbands is given by $\frac{3\hbar^2\pi^2}{2m_\perp L^2}$ (here $m_\perp$ is the effective mass in the out-of-plane direction, and $\hbar$ the reduced Planck constant). From the slope of the fitting, we estimate that $m_\perp \sim 0.22\ m_e$. We note that the measured E_{12} values are smaller by a factor of ~2 than those from the first-principle calculations; this discrepancy may arise from the anharmonicity of the bands, and/or neglecting the electronic interactions filling the first subband in our first-principles calculations.

To further characterize the second subband, we measure $R(n, B)$, where $n=\frac{C_{Tg}V_{Tg}+C_{Bg}V_{Bg}}{2e}$ is the total charge density, while keeping the perpendicular displacement field $E_\perp=\frac{C_{Tg}V_{Tg}-C_{Bg}V_{Bg}}{2\varepsilon_0}$ zero (Fig. 2a). Here, C_{Tg} and C_{Bg} are the capacitances per unit area between the two gates and InSe, e is the electron charge, and ε_0 is the permittivity of vacuum. A prominent feature revealed by the high mobility sample is the abrupt change in the slopes of the Landau fan originating from the first

band at n_{on}, as outlined by the dotted line in Fig. 2a. This change in slope reflects the onset of multi-band transport: the total charge density is now divided between two bands, in proportion to their respective density of states (DOS) $\frac{m_i^*}{\pi\hbar^2}$, where m_i^* is the in-plane effective mass of the i-th subband. Within the effective mass approximation, the charge densities residing in the two subbands are $n_1 = (n - n_{on})\frac{m_1^*}{m_1^*+m_2^*} + n_{on}$ and $n_2 = (n - n_{on})\frac{m_2^*}{m_1^*+m_2^*}$. Thus, the Landau fan from the first subband experiences a slope enhancement by a factor of $\frac{m_1^*+m_2^*}{m_1^*}$. It follows that from the ratio of the slopes, we can extract the ratio of the effective masses, which is estimated to be $m_2^*/m_1^* \sim 1.9$; using $m_1^*=0.14m_e$, as determined in prior reports[10, 13] and first principles calculations (m_e is the rest mass of the electron), we obtain that $m_2^* \sim 0.27m_e$, which is significantly enhanced with respect to that of the first subband. This enhancement is qualitatively consistent with the first-principles calculations.

A distinguishing characteristic of few-layer InSe is its large tunable Rashba SOC strength. as we have demonstrated previously[10]. To explore the SOC in the second subband, we examine the Landau fan $R(n_{tg}, B)$ of a 9-layer device that displays prominent beating in the SdH oscillations in both subbands (Fig. 2b). Here n_{tg} is the total charge density induced by top gate voltages, while the back gate is maintained at 0 V. Such beating arises from the interference of the cyclotron orbits of the inner and outer helical bands with different cross-sectional areas of the Fermi surfaces[10, 20, 21]. Fig. 2c plots the Fourier transform of the data, showcasing the two distinct frequencies for both subbands. Their Rashba SOC strengths can be measured from the beating patterns, $\alpha \approx \frac{\hbar^2}{m^*}\sqrt{\frac{\pi}{2}}\frac{\Delta n}{\sqrt{n_{avg}}}$, where $\Delta n = (e/h)B_{F,beat}$ is the density difference between the electrons in the outer and inner helical bands, n_{avg} is their average, and $B_{F,beat}$ is the beating frequency in the SdH oscillations. Using Eq. (1), we extract the values of α, which vary as a function of n_{tg}. The variations in α arises from the varying displacement field $E_\perp$. Fig. 2d plots $\alpha(E_\perp)$, demonstrating that the Rashba SOC of the second subband exhibits a much stronger dependence on $E_\perp$ than that of the first. To the best of our knowledge, this is the first demonstration of electronic filling of the second subband in a 2D vdW semiconductor, as well as the first measurement of its effective mass and tunable Rashba SOC.

To illustrate tunability of the inter-subband transition, we first examine the background-subtracted $R(n_{tg}, B)$ data from a 10-layer device, which are taken with V_{bg} maintained at 78V and 47V, respectively, hence at varying $E_\perp$ (Fig. 3a-b). The onset of the second subband, indicated by the arrows, occurs at noticeably different densities. To better characterize the electric control of the onset density's dependence on $E_\perp$, we measure the background-subtracted R as a function of both n and $E_\perp$ for an 8-layer device in the quantum Hall (QH) regime at a constant B (Fig.s 3c-d). Below n_{on}, the horizontal stripes correspond to the spin-degenerate QH states from the first subband. With the onset of the second subband, which occurs at $n=4.8$ and 7.2×10^{12} cm^{-2} at $B=7.5$T and 5T, respectively, an intricate pattern emerges, beyond the simple crossings between LLs arising from the two subbands. Specifically, the otherwise horizontal stripes that originate from the first subband curve towards higher densities, owing to the smaller charge density that reside in the first subband under large $E_\perp$. The onset of the curvature does not occur at a constant density or displacement field; rather, it occurs at larger $E_\perp$ for higher n, as indicated by the green stars in Fig.

3d. As this onset density corresponds to the energetic separation E_{12} between the two subbands, this explicitly demonstrates that E_{12} increases with $E_\perp$.

To quantify the dependence of E_{12} on $E_\perp$, we model E_{12} (in meV)$=a|E_\perp-E_{\perp 0}|^2$, and calculate the DOS from the two subbands as a function of n and $E_\perp$ at a constant magnetic field. Here a is a tunability coefficient in meV/(V/nm)^2, $E_\perp$ is in V/nm, E_{12} is in meV, and $E_{\perp 0}$ is the displacement field that minimizes E_{12}; note that $E_{\perp 0} \neq 0$ due to the broken structural inversion symmetry of InSe. Using $a \approx 85$, we calculate the DOS from the two subbands as a function of n and $E_\perp$ at a constant magnetic field. The simulation of the 8-layer device at B=5T is shown in Fig. 3e, which nicely reproduces the experimental data in Fig. 3c. Repeating the same simulation, we find that $a \approx 140$ and 210 for 9-layer and 10-layer devices, respectively. Our first-principles calculations also show a similar trend of displacement field dependent E_{12} and its enhancement with thickness. To better appreciate the magnitude of this tuning of subband separations, we plot the magnitude of E_{12} vs $E_\perp$ for 8-, 9-, and 10-layer devices in Fig. 3f; the percentage changes normalized to their respective minima are shown in Fig. 3g. The dependence of the tunability coefficient a on layer number is shown in Fig. 3f inset. Evidently, the $E_\perp$-controlled tuning effect is dramatic, up to 250 meV or over 350% at $E_\perp$=1 V/nm for the 10-layer device. Such giant tunability is hitherto unobserved, and orders of magnitude higher than any prior reports in 2D electron systems.

Lastly, we explore the LL crossings between the first and second subbands under high magnetic fields, where the interplay between the subband and spin degrees of freedom gives rise to a sequence of field-controllable electronic quartets. Fig. 4a displays the background-subtracted $R(n_{tg}, B)$ of a 10-layer device under B up to 40T. Similar to Fig.s 1-3, two sets of Landau levels are observed. The crossings between LLs from the first subband and the first LL from the second subband form a sawtooth-like structure, similar to those observed in multilayer graphene[22, 23] and GaAs systems[24, 25], evolving into ring-like patterns at higher magnetic field. These "rings" arise from a mechanism analogous to quantum Hall ferromagnetism, when electrons transfer between LLs to form a spin-polarized or spin-helical QH state that minimizes their total energy. This effect is illustrated on Fig. 4b. In regime S, the $|+,1\rangle$ and $|-,1\rangle$ LLs of the 1st subband are filled, whereas in regime P the $|+,2\rangle$ and $|-,2\rangle$ LLs of the 2nd subband are filled. Here +/- refer to the inner and outer helical bands split by the combined effects of Rashba SOC and Zeeman. In region Q the $|+,1\rangle$ and $|+,2\rangle$ LLs are filled, and the electron-electron interactions enlarge and distort this regime, where the exchange energy becomes comparable to the energy difference between $|+,2\rangle$ and $|-,1\rangle$ or $|-,2\rangle$ and $|+,1\rangle$ LLs at single-particle level.

Interestingly, we can switch between the subband-polarized and spin-helical QH states solely by varying $E_\perp$ (Fig. 4c). The red-highlighted (green-highlighted) areas in dashed outlines correspond to v=1 (v=N) of the second (first) subband, and are subband-polarized. By varying electric field, we can switch into and out of the spin-helical QH states, hence performing purely electrical control of spin texture.

In conclusion, we demonstrated population of the first and second electronic subbands in ultrathin InSe quantum wells, and determined the effective mass and the Rashba SOC strengths of both subbands. In a high magnetic field, crossings between Landau levels arising from these two subbands give rise to quantum Hall quartets, which are distorted by electron-electron interactions and tunable can be tuned by B, n and $E_\perp$. Importantly, we demonstrate via an all-electrical means

that the energetic separations and interband transitions between the first and the second subband can be modulated by an unprecedented extent, that is more than 350% in a 10-layer device. Such giant gate-tunable intersubband transitions will find wide applications in electronic and optoelectronic technologies.

Acknowledgement

References

[1]   M. S. Vitiello, G. Scalari, B. Williams, and P. De Natale, Quantum cascade lasers: 20 years of challenges, *Optics Express* **23,** 5167 (2015).

[2]   P. Schmidt, F. Vialla, S. Latini, M. Massicotte, K.-J. Tielrooij, S. Mastel, G. Navickaite, M. Danovich, D. A. Ruiz-Tijerina, C. Yelgel, V. Fal'ko, K. S. Thygesen, R. Hillenbrand, and F. H. L. Koppens, Nano-imaging of intersubband transitions in van der Waals quantum wells, *Nat. Nanotech.* **13,** 1035 (2018).

[3]   J. Zultak, S. J. Magorrian, M. Koperski, A. Garner, M. J. Hamer, E. Tóvári, K. S. Novoselov, A. A. Zhukov, Y. Zou, N. R. Wilson, S. J. Haigh, A. V. Kretinin, V. I. Fal'ko, and R. Gorbachev, Ultra-thin van der Waals crystals as semiconductor quantum wells, *Nat. Commun.* **11,** 125 (2020).

[4]   Z. R. Kudrynskyi, J. Kerfoot, D. Mazumder, M. T. Greenaway, E. E. Vdovin, O. Makarovsky, Z. D. Kovalyuk, L. Eaves, P. H. Beton, and A. Patanè, Resonant tunnelling into the two-dimensional subbands of InSe layers, *Communications Physics* **3,** 16 (2020).

[5]   K. Takeyama, R. Moriya, S. Okazaki, Y. Zhang, S. Masubuchi, K. Watanabe, T. Taniguchi, T. Sasagawa, and T. Machida, Resonant Tunneling Due to van der Waals Quantum-Well States of Few-Layer WSe2 in WSe2/h-BN/p+-MoS2 Junction, *Nano Lett.* **21,** 3929 (2021).

[6]   G. W. Mudd, M. R. Molas, X. Chen, V. Zólyomi, K. Nogajewski, Z. R. Kudrynskyi, Z. D. Kovalyuk, G. Yusa, O. Makarovsky, L. Eaves, M. Potemski, V. I. Fal'ko, and A. Patanè, The direct-to-indirect band gap crossover in two-dimensional van der Waals Indium Selenide crystals, *Scientific Reports* **6,** 39619 (2016).

[7]   G. W. Mudd, S. A. Svatek, T. Ren, A. Patane, O. Makarovsky, L. Eaves, P. H. Beton, Z. D. Kovalyuk, G. V. Lashkarev, Z. R. Kudrynskyi, and A. I. Dmitriev, Tuning the Bandgap of Exfoliated InSe Nanosheets by Quantum Confinement, *Advanced Materials* **25,** 5714 (2013).

[8]   S. Lei, L. Ge, S. Najmaei, A. George, R. Kappera, J. Lou, M. Chhowalla, H. Yamaguchi, G. Gupta, R. Vajtai, A. D. Mohite, and P. M. Ajayan, Evolution of the Electronic Band

Structure and Efficient Photo-Detection in Atomic Layers of InSe, *ACS Nano* **8,** 1263 (2014).

[9] A. Milutinović, Z. Ž. Lazarević, M. Jakovljević, B. Hadzić, M. Petrović, M. Gilić, W. D. Dobrowolski, and N. Ž. Romčević, Optical properties of layered III–VI semiconductor γ-InSe:M (M=Mn, Fe, Co, Ni), *Journal of Physics and Chemistry of Solids* **89,** 120 (2016).

[10] D. Shcherbakov, P. Stepanov, S. Memaran, Y. Wang, Y. Xin, J. Yang, K. Wei, R. Baumbach, W. Zheng, K. Watanabe, T. Taniguchi, M. Bockrath, D. Smirnov, T. Siegrist, W. Windl, L. Balicas, and C. N. Lau, Layer- and Gate-tunable Spin-Orbit Coupling in a High Mobility Few-Layer Semiconductor, *Sci. Adv.* **7,** eabe2892 (2021).

[11] J. Zeng, S.-J. Liang, A. Gao, Y. Wang, C. Pan, C. Wu, E. Liu, L. Zhang, T. Cao, X. Liu, Y. Fu, Y. Wang, K. Watanabe, T. Taniguchi, H. Lu, and F. Miao, Gate-tunable weak antilocalization in a few-layer InSe, *Phys. Rev. B* **98,** 125414 (2018).

[12] J. Zhou, J. Shi, Q. Zeng, Y. Chen, L. Niu, F. Liu, T. Yu, K. Suenaga, X. Liu, J. Lin, and Z. Liu, InSe monolayer: synthesis, structure and ultra-high second-harmonic generation, *2D Mater.* **5,** 025019 (2018).

[13] D. A. Bandurin, A. V. Tyurnina, G. L. Yu, A. Mishchenko, V. Zólyomi, S. V. Morozov, R. K. Kumar, R. V. Gorbachev, Z. R. Kudrynskyi, S. Pezzini, Z. D. Kovalyuk, U. Zeitler, K. S. Novoselov, A. Patanè, L. Eaves, I. V. Grigorieva, V. I. Fal'ko, A. K. Geim, and Y. Cao, High electron mobility, quantum Hall effect and anomalous optical response in atomically thin InSe, *Nat. Nanotech.* **12,** 223 (2017).

[14] J. Jiang, L. Xu, C. Qiu, and L.-M. Peng, Ballistic two-dimensional InSe transistors, *Nature* (2023).

[15] D. Shcherbakov, J. Yang, S. Memaran, K. Watanabe, T. Taniguchi, D. Smirnov, L. Balicas, and C. N. Lau, Quantum Hall effect in a two-dimensional semiconductor with large spin-orbit coupling, *Phys. Rev. B* **106,** 045307 (2022).

[16] S. Sucharitakul, N. J. Goble, U. R. Kumar, R. Sankar, Z. A. Bogorad, F.-C. Chou, Y.-T. Chen, and X. P. A. Gao, Intrinsic Electron Mobility Exceeding 10(3) cm(2)/(V s) in Multilayer InSe FETs, *Nano Letters* **15,** 3815 (2015).

[17] Z. Yang, W. Jie, C.-H. Mak, S. Lin, H. Lin, X. Yang, F. Yan, S. P. Lau, and J. Hao, Wafer-Scale Synthesis of High-Quality Semiconducting Two-Dimensional Layered InSe with Broadband Photoresponse, *ACS Nano* **11,** 4225 (2017).

[18] H.-C. Chang, C.-L. Tu, K.-I. Lin, J. Pu, T. Takenobu, C.-N. Hsiao, and C.-H. Chen, Synthesis of Large-Area InSe Monolayers by Chemical Vapor Deposition, *Small* **14,** 1802351 (2018).

[19] S. Tran, J. Yang, N. Gillgren, T. Espiritu, Y. Shi, K. Watanabe, T. Taniguchi, S. Moon, H. Baek, D. Smirnov, M. Bockrath, R. Chen, and C. N. Lau, Surface transport and quantum Hall effect in ambipolar black phosphorus double quantum wells, *Sci. Adv.* **3,** e1603179 (2017).

[20] Y. A. Bychkov, and E. I. Rashba, Properties of a 2D electron gas with lifted spectral degeneracy, *JETP* **39,** 78 (1984).

[21] J. Nitta, T. Akazaki, H. Takayanagi, and T. Enoki, Gate Control of Spin-Orbit Interaction in an Inverted In0.53Ga0.47As/In0.52Al0.48As Heterostructure, *Phys. Rev. Lett.* **78,** 1335 (1997).

[22] P. Stepanov, Y. Barlas, T. Espiritu, S. Che, K. Watanabe, T. Taniguchi, D. Smirnov, and C. N. Lau, Tunable Symmetries of Integer and Fractional Quantum Hall Phases in Heterostructures with Multiple Dirac Bands, *Phys. Rev. Lett.* **117,** 076807 (2016).

[23] Y. Shi, S. Che, K. Zhou, S. Ge, Z. Pi, T. Espiritu, T. Taniguchi, K. Watanabe, Y. Barlas, R. Lake, and C. N. Lau, Tunable Lifshitz Transitions and Multiband Transport in Tetralayer Graphene, *Phys. Rev. Lett.* **120,** 096802 (2018).

[24] X. C. Zhang, D. R. Faulhaber, and H. W. Jiang, Multiple phases with the same quantized Hall conductance in a two-subband system, *Phys. Rev. Lett.* **95,** 216801 216801 (2005).

[25] X. C. Zhang, I. Martin, and H. W. Jiang, Landau level anticrossing manifestations in the phase-diagram topology of a two-subband system, *Phys. Rev. B* **74,** 073301 073301 (2006).

Figure 1. Magnetotransport data from InSe devices as a function of sample thickness. (a-c). dR/dn_{tg} vs n_{tg} and B from a single InSe sheet with regions that are 6-, 7-, and 8-layers thick. Inset: schematics of the flake. (d). Measured onset density for the second subband n_{on} as a function of the inverse layer number squared. The right axis plots the intersubband transition energy E_{12} calculated assuming a constant first subband $m^*=0.14\ m_e$. The line is a linear fit to the data points. Inset: Illustration of the subbands. (e). Band structure of 7-layer InSe with Rashba SOC obtained by first-principles calculations.
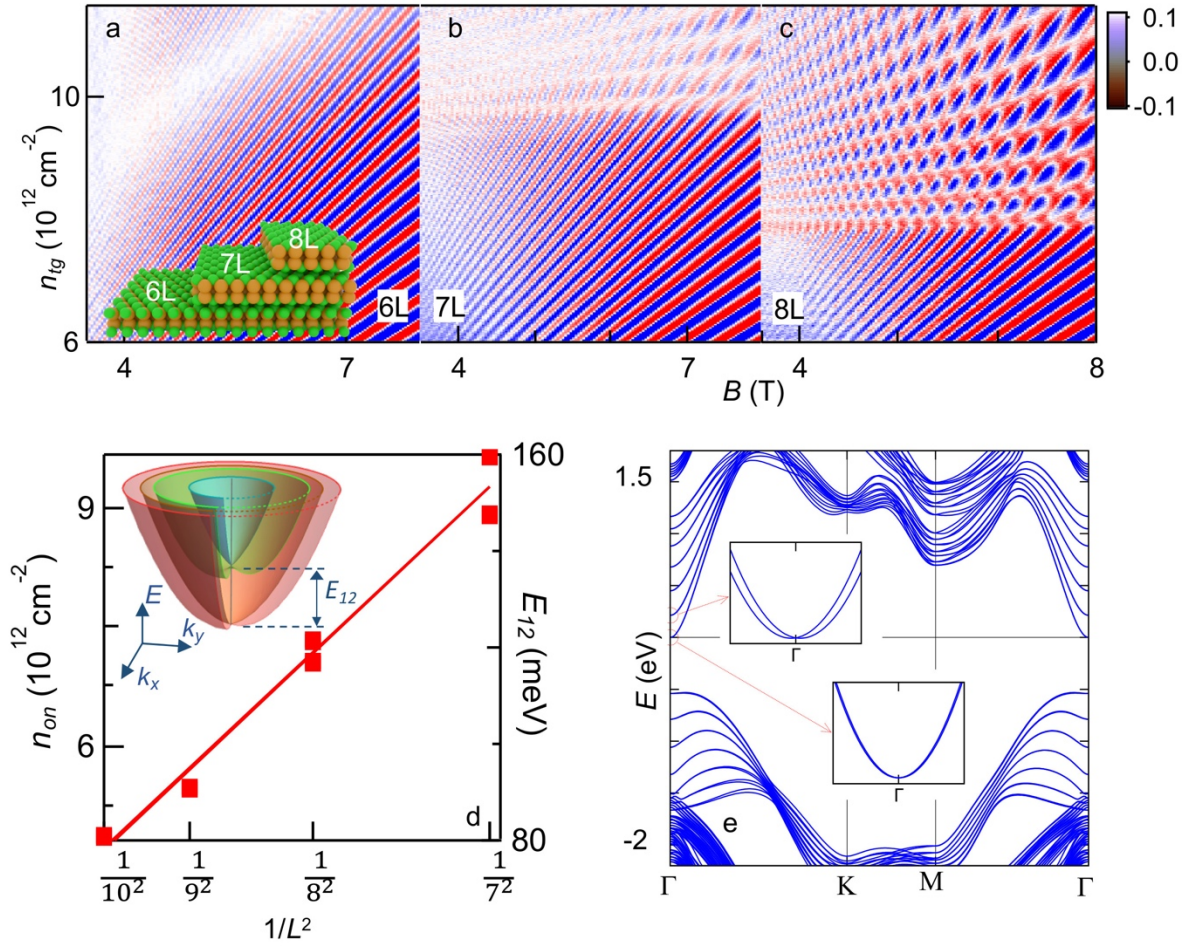
Figure 2. Measurements of the second subband's effective mass and Rashba SOC parameter. (a). $R(n, B)$ for an 8-layer device taken at $E_\perp=0$. The dotted line indicates the change in the slope of the quantum oscillations from the first subband after reaching the onset of the second subband. (b). dR/dn (n_{tg}, B) for a 9-layer device taken at $V_{bg}=80V$. (c). FFT of the oscillations in (b). The twin peaks arise from the spin-split bands due to the Rashba SOC. (d). Extracted SOC parameter α vs $E_\perp$ for the first (red) and second (blue) subband.
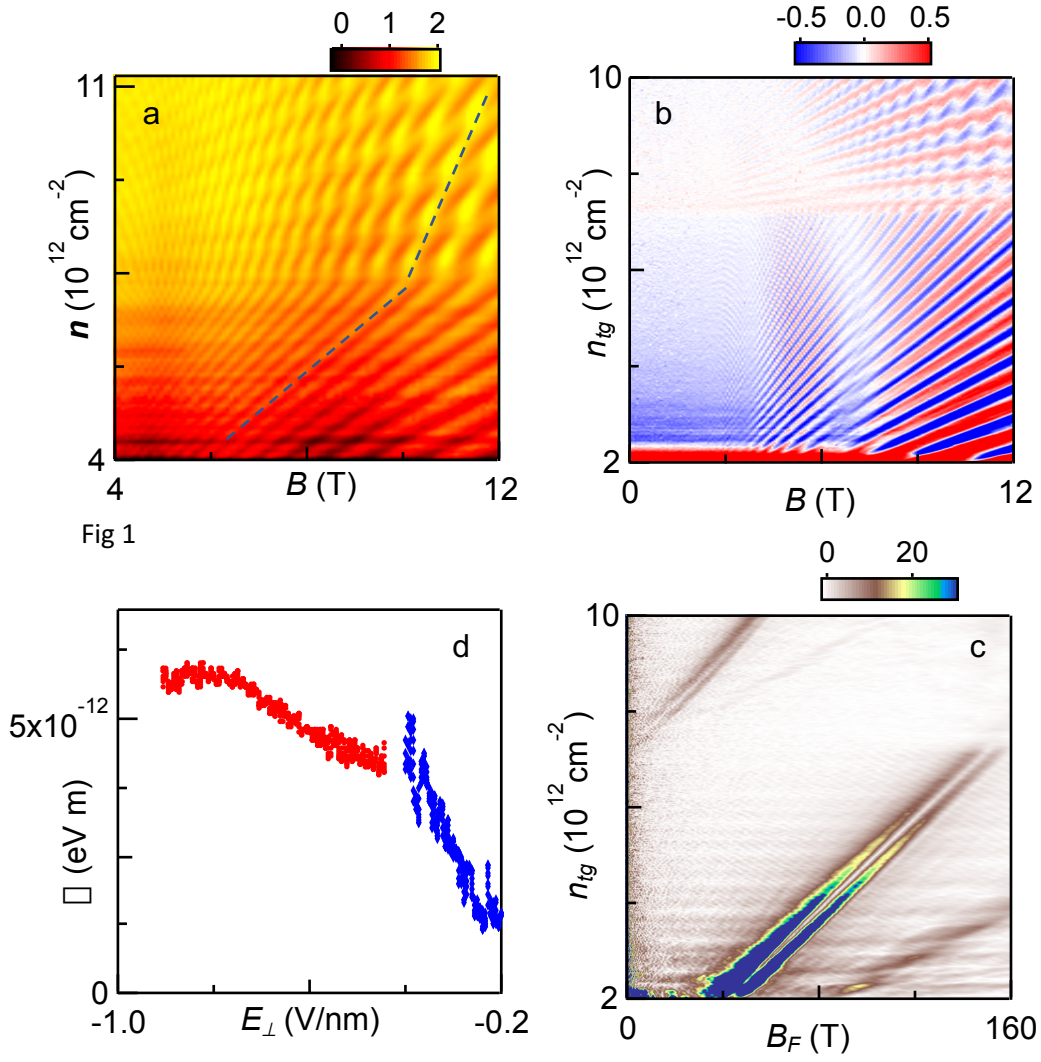

Fig 1

Figure 3. Tuning the intersubband energy with a transverse electric field $E_\perp$. (a-b). Background subtracted $R(n_{tg}, B)$ for a 10-layer device, with V_{bg} at 47 and 78V, respectively. The arrows indicate onset charge densities for the second subband. (c-d). Background-subtracted $R(n, E_\perp)$ of an 8-layer device at B=5T and 7.5 T, respectively. (e). Simulation of the density of states as a function of n and $E_\perp$ at B=5T for the 8-layer device, calculated using E_{12} (in meV)$=aE_\perp^2$, where a=85 is the tunability parameter, and $E_\perp$ is in V/nm. (f-g). Extracted intersubband spacing E_{12} and its percentage change vs $E_\perp$ for 8-layer (blue), 9-layer (green) and 10-layer (red) devices, respectively. Inset in g: the tunability parameter a as a function of layer number.
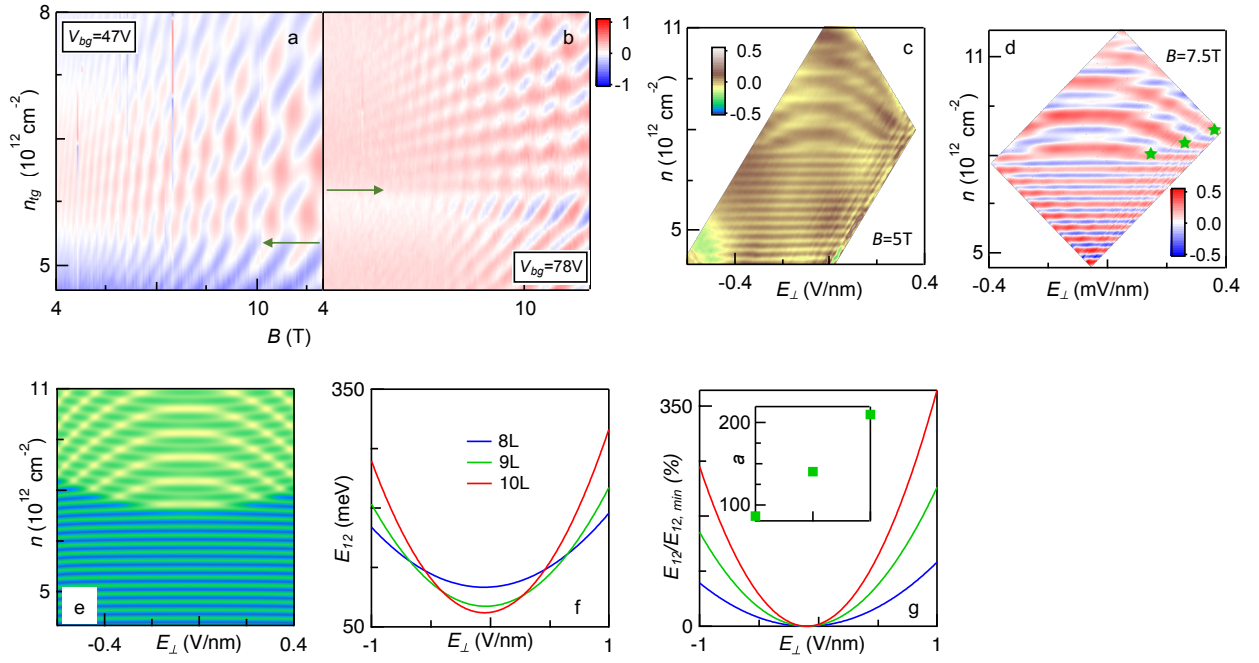
Figure 4. Quantum Hall helical-magnetism in InSe under high magnetic fields. (a). Background-subtracted $R(n_{tg}, B)$ for a 10-layer device subjected to high magnetic fields. (b). Schematic of LL crossing and formation of spin-helical quantum Hall state. (c). Background-subtracted $R(v, E_{\perp})$ at B=34.5T, showing tuning of the QH helical-magnetic states by $E_{\perp}$.